



**HAL**  
open science

# Understanding the influence of media geometry on the degradation of acrylonitrile: Experimental and CFD analysis

Henrietta Essie Whyte, Albert Subrenat, Cécile Raillard, Valérie Hequet

► **To cite this version:**

Henrietta Essie Whyte, Albert Subrenat, Cécile Raillard, Valérie Hequet. Understanding the influence of media geometry on the degradation of acrylonitrile: Experimental and CFD analysis. Chemical Engineering Science, 2019, pp.115217. 10.1016/j.ces.2019.115217 . hal-02285151

**HAL Id: hal-02285151**

**<https://hal.science/hal-02285151>**

Submitted on 12 Sep 2019

**HAL** is a multi-disciplinary open access archive for the deposit and dissemination of scientific research documents, whether they are published or not. The documents may come from teaching and research institutions in France or abroad, or from public or private research centers.

L'archive ouverte pluridisciplinaire **HAL**, est destinée au dépôt et à la diffusion de documents scientifiques de niveau recherche, publiés ou non, émanant des établissements d'enseignement et de recherche français ou étrangers, des laboratoires publics ou privés.

## Journal Pre-proofs

Understanding the influence of media geometry on the degradation of acrylonitrile: Experimental and CFD analysis

Henrietta Essie Whyte, Albert Subrenat, Cécile Raillard, Valérie Hequet

PII: S0009-2509(19)30709-2  
DOI: <https://doi.org/10.1016/j.ces.2019.115217>  
Reference: CES 115217

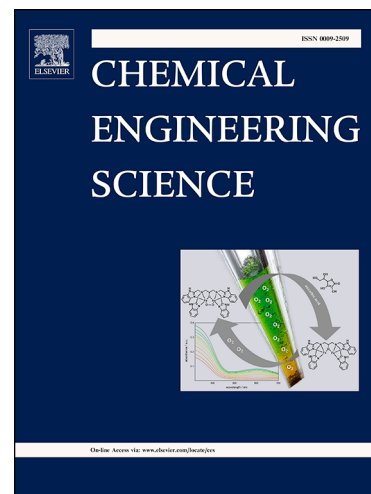
To appear in: *Chemical Engineering Science*

Received Date: 11 April 2019  
Revised Date: 23 July 2019  
Accepted Date: 7 September 2019

Please cite this article as: H. Essie Whyte, A. Subrenat, C. Raillard, V. Hequet, Understanding the influence of media geometry on the degradation of acrylonitrile: Experimental and CFD analysis, *Chemical Engineering Science* (2019), doi: <https://doi.org/10.1016/j.ces.2019.115217>

This is a PDF file of an article that has undergone enhancements after acceptance, such as the addition of a cover page and metadata, and formatting for readability, but it is not yet the definitive version of record. This version will undergo additional copyediting, typesetting and review before it is published in its final form, but we are providing this version to give early visibility of the article. Please note that, during the production process, errors may be discovered which could affect the content, and all legal disclaimers that apply to the journal pertain.

© 2019 Published by Elsevier Ltd.



**Understanding the influence of media geometry on the degradation of acrylonitrile:****Experimental and CFD analysis**

Henrietta Essie WHYTE, Albert SUBRENAT, Cécile RAILLARD, Valérie HEQUET

IMT Atlantique,-CNRS GEPEA, UMR 6144, 4 Rue Alfred Kastler CS 20722, 44307 Nantes Cedex 3, France

**\*Corresponding author: [whytehenrietta@yahoo.com](mailto:whytehenrietta@yahoo.com)**

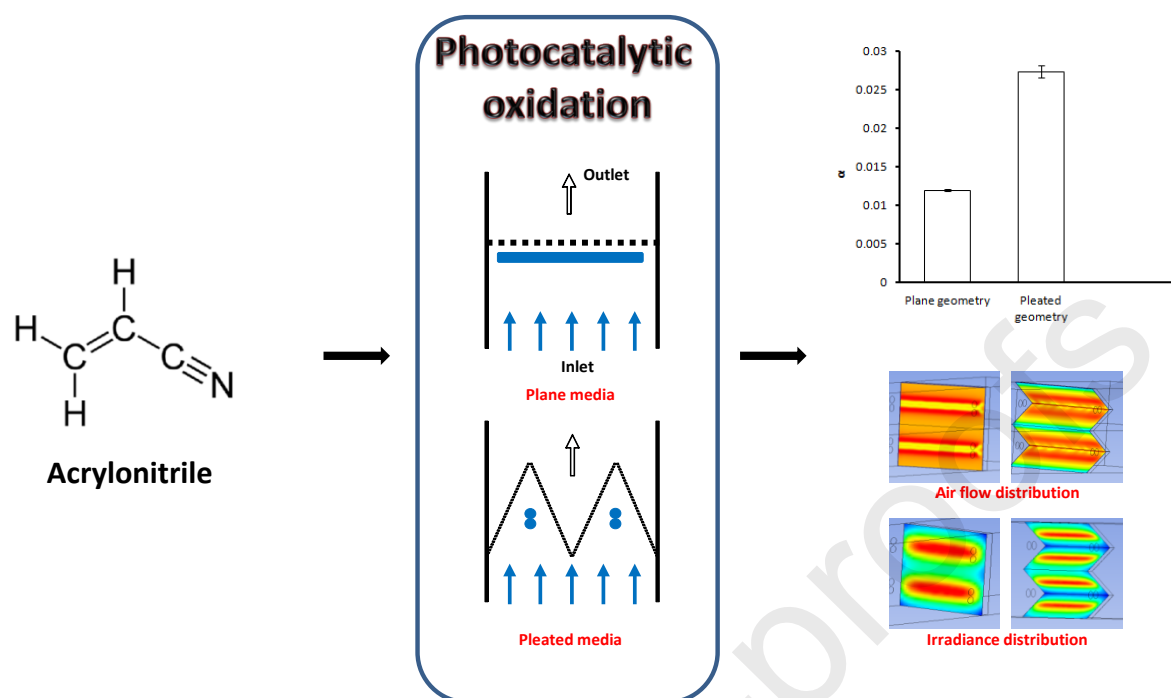
---

**ABSTRACT**

The media geometry design is a parameter that influences the efficiency of PCO device for indoor air treatment. However, there is little information in the literature to show how it impacts degradation efficiency. In this work, media geometry influence on the degradation of acrylonitrile is investigated experimentally and with numerical simulations. The experiments were conducted in a laboratory closed loop multi-pass reactor with the aim of comparing degradation efficiencies using plane and pleated media geometries. The experimental results showed a higher removal efficiency for the pleated media. Numerical simulations provided some information to better connect the increase in efficiency to the change in media geometry considering and modeling the media as a porous zone. The simulation results showed that pollutants had lower velocity in pleated media thus contact time was increased by 76%. Additionally, the more heterogeneous distribution of velocity and irradiance in the pleated media could counteract the influence of the contact time and possibly explain the lower than expected experimental results.

**Keywords:** Photocatalytic oxidation, Indoor air treatment, Acrylonitrile, Single-pass removal efficiency, Computational fluid dynamics, Photocatalytic media geometry

## Graphical abstract



## Highlights

- The influence of plane and pleated media geometry on the photocatalytic oxidation acrylonitrile studied for the first time
- The surface corrected single-pass removal efficiency higher for pleated media than for plane media
- CFD highlights important information on air flow and irradiance distribution that help to explain experimental results

## 1 Introduction

Air treatment technologies are used to improve indoor air quality by reducing the level of pollutants and can be utilised alone or in combination with HVAC systems. Technologies that can be implemented in commercial devices for removing pollutants are mainly mechanical filtration, adsorption, ozonation, ultraviolet irradiation and photocatalytic oxidation (PCO). These technologies control pollutants and allow air quality levels to be maintained with reduced outdoor air supply and concomitant energy savings (Bergeron et al., 2007; Le et al., 2015; Perraud et al., 1992; Rosenbaum et al., 2004; Schoenleber et al., 2007). These devices can be considered for use in hospitals operating rooms (OR). The OR air may contain different types of pollutants (chemical gases, biological contaminants and particulate matter) due to specific activities (disinfection, cleaning, surgical process and anesthesia) that are performed (Barrett and Garber, 2003; Dascalaki et al., 2008). Among the different air cleaning technologies used for the removal of gaseous chemical pollutants, photocatalytic oxidation seems to be more and more employed.

Photocatalytic oxidation is an advanced oxidation process that uses a catalyst (often  $\text{TiO}_2$ ) and UV light to decompose a broad spectrum of Volatile Organic Compounds (VOCs) into innocuous final products like  $\text{CO}_2$  and  $\text{H}_2\text{O}$ . The performance of PCO is affected by several factors such as air velocity, light intensity, initial concentration, relative humidity, and presence of co-pollutants. The influence of these key parameters has been greatly studied in the literature (Ao et al., 2004; Chen and Zhang, 2016; Dillert et al., 2012; Kozlov et al., 2003; Pichat, 2010; Raillard et al., 2004; Sleiman et al., 2009; Ye et al., 2006; Yu and Brouwers, 2009). However, the influence of the media geometry has not been greatly explored.

For the same reactor volume, the performance of the degradation can be increased by modifying the media geometry such that it (i) has a high surface area to allow contact with as large a

quantity of reactants as possible, (ii) allows a better utilization of the light and (iii) allows a longer contact time between the reactants and the photocatalyst (Birnie et al., 2006). Destailats et al. (Destailats et al., 2012) studied the degradation of seven VOCs using plane media geometry and a pleated media geometry whilst Batault (Batault, 2014) studied the influence of plane and pleated geometry on the degradation of toluene. Both authors noticed an increase in the degradation efficiency when the media geometry was changed from a plane to a pleated configuration. They attributed the difference in performance of the two configurations to difference in (i)  $\text{TiO}_2$  content, (ii) contact time within media and (iii) irradiance distribution within media. Whilst Destailats *et al.* (Destailats et al., 2012) suggested that the increase in contact time is as a result of the decreasing velocity of pollutants within the pleated media, Batault (Batault, 2014), suggested that the increase in the contact time is as a result of the longer path length travelled by the pollutants when the media was changed from plane to pleated. Additionally, both authors agreed that for the same average light intensity received on the photocatalytic media (plane and pleated), a modification of the irradiance distribution can also have an influence on the global efficiency of the PCO. These parameters are difficult to measure or confirm experimentally. An effective approach to solve this issue is through the use of Computational Fluid Dynamics (CFD).

CFD is a useful tool to investigate photocatalytic reactors for air treatment (Boyjoo et al., 2013). It allows for comprehensive analysis of photocatalytic reactor through the simulation of fluid dynamics, species mass transport, chemical reaction kinetics, and irradiance distribution. It is also a cost effective approach as it helps to reduce the number of experiments necessary to predict the behavior of a process.

Mohseni and Taghipour (Mohseni and Taghipour, 2004) used experimental and CFD modeling to investigate the flow field and the photocatalytic degradation of vinyl chloride in an annular reactor and reported good agreement of conversion values between the model to experimental

results. Castrillion and de Lasa (Romero-Vargas Castrillón et al., 2006) used CFD to simulate the flow field in a photo-CREC reactor. The simulated flow field enabled them to uniformize mass flow and contact time distributions within the reactor. Salvado-Estivill *et al.* (Salvadó-Estivill et al., 2007) modeled the degradation of trichloroethylene in a single-pass flat plate photocatalytic reactor by combining CFD modeling of the fluid flow in the reactor with radiation field modeling and photocatalytic reaction kinetics. A comparison of the model prediction with the experimental results yielded good results (Salvadó-Estivill et al., 2007). Chong *et al.* (Chong et al., 2011) modeled flow field, radiation and kinetics of toluene and formaldehyde through a porous monolith photocatalytic reactor. The simulation gave them information about the local flow field and light intensity profile. They also observed a good agreement between model predictions and experimental values for conversion profiles. Wang *et al.* (Wang et al., 2014) conducted a CFD simulation to enable them describe the local UV flux within a porous monolith channel. They also investigated the monolith to lamp spacing and the number of lamps to achieve the optimal configuration that would provide higher formaldehyde conversion yields. The results of the model were compared experimentally in a corrugated wall, bench scale reactor constructed in the laboratory. Passalia *et al.* (Passalia et al., 2012) used a methodology based on previously determined kinetic parameters of a simple geometry, continuous reactor and applied them to a corrugated wall reactor to predict its performance for the degradation of formaldehyde. Their results showed that the kinetic expression obtained was independent of the chosen reactor geometry and size. They found that the overall pollutant conversion showed good agreement between model predictions and experiments, with a root mean square error less than 4%. Using CFD helped them with the simulation and resolution of velocity and concentrations fields in a complex geometry reactor that otherwise would have been more difficult to achieve. Queffeuilou *et al.* (Queffeuilou et al., 2010) were able to successfully use CFD to predict and validate the performance of a batch

reactor for the removal of acetaldehyde. With their proposed model, they found that the predicted times of acetaldehyde removal are of the same order magnitude than those obtained experimentally.

To the best of the authors' knowledge no study has been done on using CFD to explain the influence of the change of media geometry on the degradation efficiency of a pollutant.

In this work, the influence of media geometry on the degradation of acrylonitrile is studied for the first time. Acrylonitrile is a compound of concern found in surgical smoke, one of the main pollutants in an OR. Numerical simulations by CFD are also conducted to better understand the influence of the change of media geometry on the efficiency in terms of the air flow and light irradiance.

## 2 Materials and methods

### 2.1 Experimental Set-up

The experimental set-up used in this study is presented in Fig. 1. It consists of the VOC generation bench, the photocatalytic reactor and the sampling and analytical devices.

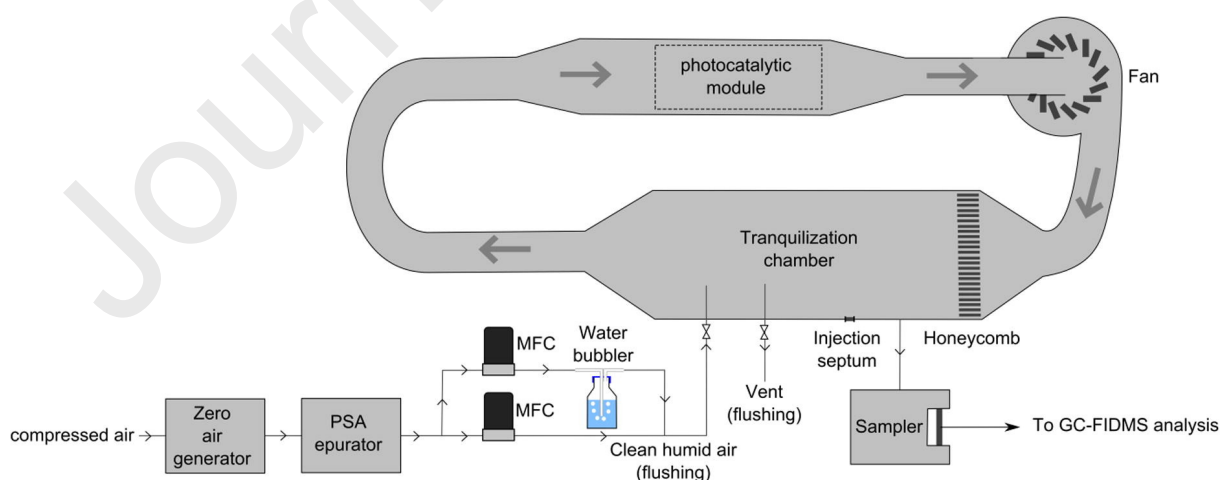


**Fig. 1 : Schematic representation of the closed-loop photocatalytic reactor**

### 2.1.1 Generation of pollutant concentrations

To generate the desired concentration of acrylonitrile, the process started first by generating clean humid air. To do this, compressed air from the laboratory network was passed through an air zero generator Claind AZ 2020 to eliminate VOCs present in the air, then through a Pressure Swing Adsorption (PSA) device remove humidity as well as CO<sub>2</sub>. The air is then humidified to 50 % by bubbling it through a water bottle at an average room temperature of 20°C. Acrylonitrile (C<sub>3</sub>H<sub>3</sub>N) was supplied by *Air products* in certified commercial gas cylinder balanced in nitrogen at 150 bars. Acrylonitrile is mixed with the humid air zero to dilute it before injection into the reactor. The desired concentration of 2 ppm is achieved by adjusting the gas flow rates using mass flow controllers (MFC).

### 2.1.2 Photocatalytic reactor

The reactor that was used to perform experiments is a 420-L multi-pass reactor that has been described in previous articles (Batault et al., 2017; Maudhuit et al., 2011; Raillard et al., 2014; Whyte et al., 2018). It is a closed-loop reactor built made up entirely of stainless steel to minimize surface losses of pollutants. It is equipped with a variable speed fan which is used to control the air flow in the reactor and allows a flow rate from 28 to 300 Nm<sup>3</sup>.h<sup>-1</sup>. For the present study, the flow was set at 148 Nm<sup>3</sup>.h<sup>-1</sup>. The reactor also has a tranquilization chamber from where the pollutants are introduced into the reactor and sampling is done. A honeycomb is placed at the inlet of the chamber to provide a homogeneous flow distribution. The photocatalytic media and UV lamps are housed in the photocatalytic module. A Quartzel<sup>®</sup> photocatalytic media was used in this work. It is a commercial media by Saint-Gobain Quartz. It consists of SiO<sub>2</sub> fibers coated with TiO<sub>2</sub> deposited through a sol-gel method and pressed into a felt with average thickness of 17.5 ± 1.5 mm. The BET specific surface area was measured at 112 ± 1 m<sup>2</sup>.g<sup>-1</sup> with a Micrometrics ASAP 2020 by N<sub>2</sub> adsorption. The media was irradiated by two 18-W UVC fluorescent tubes (Phillips TUV PL-L series). A Vilber Laurmat VLX-3W

radiometer equipped with a calibrated CX-254 nm sensor was used to measure the irradiance over the entire photocatalytic media surface. The average light intensities were achieved by using a variable voltage supply to modify the power of the lamps. In this work, the light intensity was maintained at an average of  $4.5 \text{ mW}\cdot\text{cm}^{-2}$ . Prior to each experimental run, the reactor and photocatalytic media were cleaned by flushing with humid zero air under UV irradiation for several hours.

Two photocatalytic media geometries were used in this work; plane and pleated. For the plane media configuration (Fig.2), the photocatalytic media has a square surface with an area of  $0.04 \text{ m}^2$ . The media is placed perpendicularly to the flow whilst the lamps are placed horizontally to media and are also 3 cm away from the media surface. The pleated configuration consists of the photocatalytic media folded into four pleats creating two triangles at  $60^\circ$  with a surface area of  $0.072 \text{ m}^2$ . The lamps are placed vertically within the triangles. The lamps were also placed 3 cm from the middle of the media pleats.

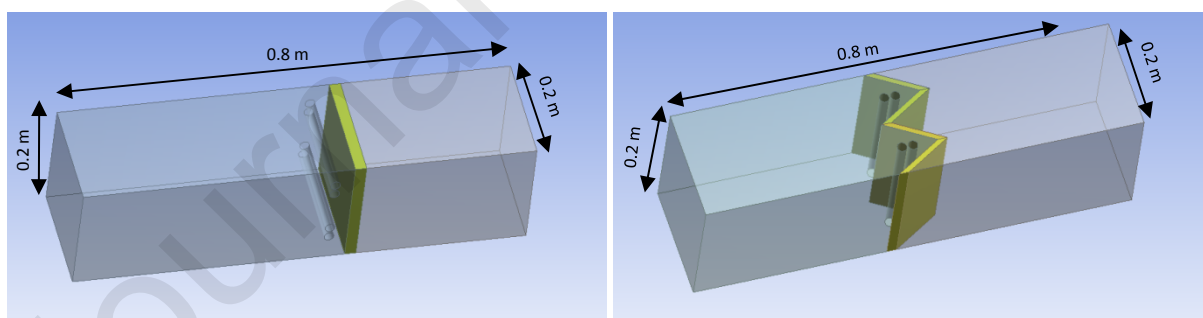


**Fig. 2: Representation of the photocatalytic module showing position and arrangement of lamps and media for the plane (left) and pleated (right) media configuration**

### 2.1.3 Sampling and analytical methods

To monitor acrylonitrile concentrations over the period of the degradation, samples were taken onto stainless-steel cartridges packed with Carboxen 100 (Perkin Elmer). The Automatic Clean Room Sampling System (ACROSS) by Tera Environnement was used to sample at a rate of

200 mL.min<sup>-1</sup> for 2.5 min. The analysis was carried out using a Thermal Desorber/Gas Chromatograph/Flame Ionization Detector/Mass Spectrometer (TD/GC/FID/MS). The column used in the GC was a polar column from Restek (Rxi-624Sil MS) which was connected to a FID for the quantification of compounds and a MS for the identification of compounds. The TD/GC/FID/MS analysis conditions are described in Table 1. The limits of detection was calculated by multiplying the background noise by 3. It was calculated as 0.1 ppm for isoflurane and 0.075 ppm for acrylonitrile.

Step	Parameter	Value
<b>Tube desorption</b>	Desorption temperature	250°C
	Desorption time	10 min
<b>Trap desorption</b>	Focusing trap temperature	-30°C
	Desorption temperature	250°C
	Transfer line temperature	250°C
<b>FID</b>	Temperature (°C)	250
	Fuel	H <sub>2</sub>
	Flow rate (mL.min <sup>-1</sup> )	45
	Oxidizer	Air
<b>MS detection</b>	Flow rate (mL.min <sup>-1</sup> )	450
	Source temperature (°C)	200
	Electron Energy (eV)	70
	Scan range (m/z)	20-200
<b>GC</b>	Column	Rxi-624SilMS (60m x 0.35mm x 1.8µm)
	Oven temperature program	35°C (5min), 15°C.min <sup>-1</sup> to 150°C (2 min), 20°C.min <sup>-1</sup> to 250°C (5 min)

**Table 1 : TD/GC/FID/MS analysis conditions**

## 2.2 Calculating the single-pass removal efficiency

In this work, the indicator that was chosen to compare the efficiency of the plane and pleated media configurations is the single-pass removal efficiency. The reactor used in this work is a multi pass reactor which provides information on the concentration degradation profiles over

the entire duration of the experiment. It however does not provide direct information on the single-pass removal efficiency. This indicator has to be determined indirectly by employing mathematical models. In this work the model that is used has been developed by Dumont and Héquet is explained in their paper (Dumont and Héquet, 2017). The model, describes a first order decay relationship of concentration vs. time in a closed-loop reactor with a global apparent kinetic constant, including chemical kinetics and reactor dynamics. The model does not explicitly account for the light effect or the diffusion phenomena and is given as follows:

$$C = C_0 \exp\left[-\frac{t}{\tau_R} \left[1 - \exp(-\alpha)\right]\right] \quad (1)$$

In Eq. (1) the term  $\alpha$  is the single-pass removal efficiency and represents the fraction of the total flow treated during the time  $\tau_R$  (residence time in the reactor).  $C$  is the pollutant concentration at time  $t$  and  $C_0$  is the initial pollutant concentration. Numerical resolutions were carried out using Excel<sup>®</sup> Solver which is based on the least-square method.

### 2.3 CFD Model Development

The simulation was done using the commercial software ANSYS 14.5. The geometry was defined to meet the dimensions and characteristics of the photocatalytic module of the closed-loop reactor using ANSYS design modeler. The photocatalytic reactor volume was discretized into 503123 structured and unstructured cells. This number of cells was found to be high enough to give mesh-independent results and provided a satisfactory capture of the flow and irradiance qualities at a reasonable computational time.

#### 2.3.1 Fluid dynamics

The simulation of fluid dynamics in the photocatalytic module was performed considering a three dimensional, steady state turbulent flow. The fluid was air and was considered as

incompressible and isothermal with constant physical properties. The photocatalytic media was simulated as a porous zone. The conservation of mass is achieved by solving the classical continuity equation. For the conservation of momentum, since the flow is in the turbulent regime, the Reynolds-Averaged Navier Stokes (RANS) equation is solved. However since the reactor also contains a porous region which is the photocatalytic media, the equations are modified to account for the porosity of the media. The modified continuity and the momentum equations are given below as Eq. (2) and Eq. (3) respectively (ANSYS Inc., 2013; Wang et al., 2014).

$$\frac{\partial(\varepsilon\rho)}{\partial t} + \nabla(\varepsilon\rho\vec{v}) = 0 \quad (2)$$

$$\frac{\partial(\varepsilon\rho\vec{v})}{\partial t} + \nabla(\varepsilon\rho\vec{v}\vec{v}) = -\varepsilon\nabla p + \nabla\varepsilon\rho g + \nabla\varepsilon\tau + S_M \quad (3)$$

where  $\rho$ ,  $v$ ,  $\tau$ ,  $g$ ,  $p$  and  $\varepsilon$  are the density of the fluid, the velocity of the fluid, stress tensor, gravity, pressure and porosity of the media respectively.  $S_M$  is the momentum sink term which accounts for the loss of momentum or pressure drop due to an obstacle which in this case is the media. It is given by the modified Darcy law (Eq. (4)) as:

$$S_M = \frac{\mu}{k}v + \frac{1}{2}C\rho v^2 \quad (4)$$

where  $k$  is the permeability,  $C$  is the inertial resistance factor,  $v$  is the velocity,  $\mu$  is the dynamic viscosity. The media was assumed to be a porous body with porosity of 0.875. The permeability and inertial resistance factor are calculated  $1.45 \times 10^{-8} \text{ m}^2$  and  $823 \text{ m}^{-1}$  respectively. The parameters were calculated from experimental data. This was done by simply measuring and plotting a graph of the pressure drop as a function of velocity. By using the regression model from experimental results and the modified Darcy equation (Equation 4), the permeability and inertial resistance factor is calculated.

The inlet velocity was set as  $1\text{m}\cdot\text{s}^{-1}$  whilst at the outlet, atmospheric pressure was applied. A no-slip boundary condition was imposed at the reactor walls.

### 2.3.2 Radiation field modeling

To model the irradiance distribution within the reactor the radiative transport equation (RTE) needs to be solved. The RTE is an integro-differential equation which describes the photonic rays with their corresponding energy loss due to absorption and out-scattering and gain due to in scattering. It describes the movement of a bundle of light rays travelling in a direction  $s$  having a solid angle  $\Omega$ , and intensity  $I$ . The generic form of the equation is given in Eq. (5) as (ANSYS Inc., 2013):

$$\frac{dI(s\Omega)}{ds} + aI(s\Omega) + \sigma I(s\Omega) = an^2\frac{\sigma_{SB}T^4}{\pi} + \frac{\sigma_s}{4\pi}\int_0^{4\pi} I(s'\Omega)\phi(s'.s)d\Omega' \quad (5)$$

Where  $s$  is the direction,  $s'$  is the scattering direction,  $a$  is the absorption coefficient,  $n$  is the refractive index,  $\sigma$  is the scattering coefficient,  $\sigma_{SB}$  is the Stefan-Boltzmann constant,  $T$  is the local temperature,  $\Phi$  is the phase function,  $\Omega'$  is the scattering solid angle. Numerical resolution of the RTE was done using the discrete ordinate (DO) method which solves the RTE for a finite number of discrete solid angles, each one associated with a vector direction. When using the DO method, the spatial discretization of the computational region is taken directly from the mesh grid topology. However, the directional discretization for the RTE was explicitly specified using an angular discretization of the sphere octant of  $10 \times 10$  divisions (enough to avoid the well-known ‘‘ray effect’’) and  $3 \times 3$  pixelation (enough to overcome angle overhanging).

It is assumed that there is negligible scattering, emission or absorption by the fluid medium thus in the fluid medium Eq. (5) reduces to:

$$\frac{dI(s\Omega)}{ds} = 0 \quad (6)$$

However, there is a gradual loss of light due to absorption through the photocatalytic media. As stated in the literature (Boyjoo et al., 2013; Chong et al., 2011) for immobilized systems, the scattering and reflection are assumed to be negligible. Therefore within the photocatalytic media, Eq. (7) is reduced to:

$$\frac{dI(s\Omega)}{ds} + aI(s\Omega) = 0 \quad (7)$$

The absorption coefficient ( $a$ ) is therefore a necessary user input. It is related to the UV-Transmittance (UVT) by the Beer-Lambert Law which is given in Eq. (8) as:

$$UVT = \exp(-ax) \quad (8)$$

where  $x$  is the path length travelled by the light inside the photocatalytic media.

The UVT of the media was found to be 0.6% therefore the absorption coefficient is calculated as  $292 \text{ m}^{-1}$ .

Finally, as a boundary condition for the resolution of the RTE, a surface emission model was considered for the UV lamps, as this model has been previously found to be appropriated to represent fluorescent UV lamps (Boyjoo et al., 2014, 2013). The lamp wall was set as semi-transparent purely diffuse wall with an external irradiance. All the remaining walls except the reactor wall were set as zero-thickness and also semi-transparent. The reactor wall was defined as diffusely reflecting opaque stainless walls with a reflectivity of 0.15. The temperature was fixed to 1 K in all domains to inactivate calculations of radiation emission.

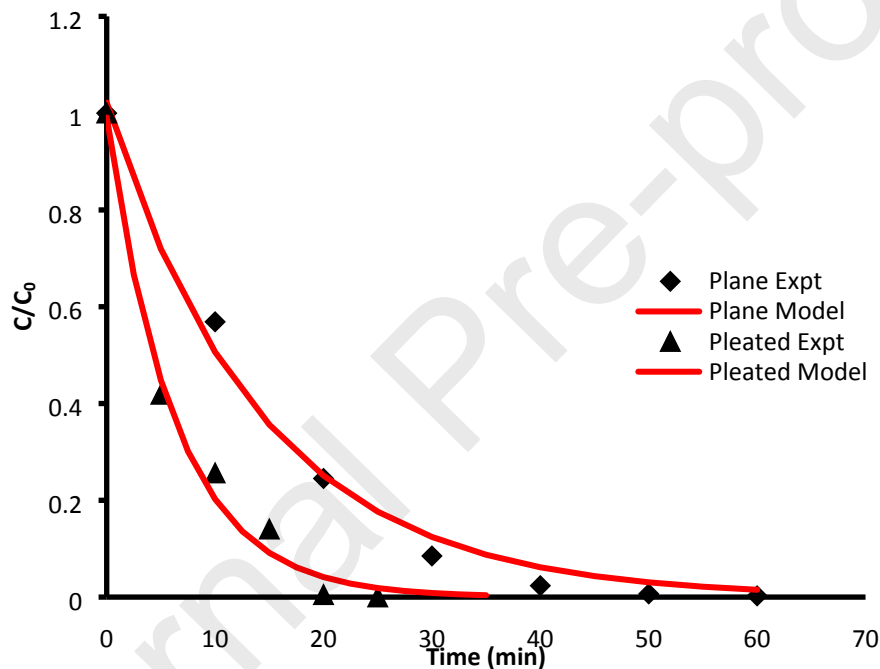
### 2.3.3 *Solution strategy and convergence criteria*

ANSYS CFX solver was used to solve the fluid dynamics equations whilst ANSYS Fluent was utilized to solve the RTE equations. The first order high resolution scheme was employed for fluid dynamics whilst the second order upwind method was used to solve the RTE. The convergence was ensured by imposing a residual value of  $10^{-6}$  for continuity and momentum and  $10^{-4}$  for incident radiation. It took 1130 iterations and 6 hours to achieve convergence for fluid dynamic modeling whilst it took 1100 iterations and about 14 hours to achieve convergence for radiation field modeling.

### 3 Results and discussion

#### 3.1 Degradation profile of acrylonitrile

Fig. 3 shows acrylonitrile degradation experimental points fitted with the model (Eq. 1) for the plane and pleated configuration. Under the experimental conditions of  $C_0 = 2$  ppm,  $v = 1$  m.s<sup>-1</sup>,  $I = 4.5$  mW.m<sup>-2</sup> and RH = 50 % the complete degradation of acrylonitrile was achieved within 60 minutes and 20 minutes for plane and pleated respectively. Both curves were characterized by a mono-exponential profile. The model was shown to fit satisfactorily to the experimental points based on the co-efficient of determination ( $R^2$ ) of 0.99. Under the experimental



conditions, the single-pass removal efficiency ( $\alpha$ ) was then calculated as 0.012 and 0.027 respectively for plane and pleated configurations. This indicated that in one pass, 1.2% of acrylonitrile would be eliminated from the total flow that passed through the plane media whilst for the pleated media 2.7% would be eliminated in one-pass.

**Fig. 3: Experimental degradation curve of acrylonitrile during use of plane and pleated media configurations fitted with model developed by Dumont and Héquet under reference experimental conditions of  $C_0 = 2$  ppm;  $v = 1$  m.s<sup>-1</sup>;  $I = 4.5$  mW.cm<sup>-2</sup>; RH = 50 %**

### *3.2 Influence of the media geometry on the single-pass removal efficiency during photocatalytic degradation of acrylonitrile*

In this work, to study the influence that the change in media geometry had on the degradation of acrylonitrile, experiments were carried out with a pleated media configuration and the results compared to reference experiments carried out with the plane media configuration. In order to further highlight the influence of the contact time, the average light intensity was kept constant for both plane and pleated media geometries. To ensure that the average light intensity received on the pleated media was the same as the plane media, numerical simulations were used and are detailed in section 3.3.2.

It was observed that the single-pass removal efficiencies increased from  $(12.08 \pm 0.11) \times 10^{-3}$  for the plane media to  $(27.42 \pm 0.74) \times 10^{-3}$  for the pleated media. It is evident that the pleated media geometry improves the PCO performance. This is in accordance with what Destailats *et al.* (Destailats et al., 2012) and Batault (Batault, 2014) observed. Three main reasons may account for this efficiency increase: (i) an increase in the surface area translates to an increase in the amount of catalyst/active sites available for pollutant removal (ii) increase in the contact time between pollutants and media (iii) better distribution of light intensity.

To eliminate the effect of the increase in catalyst quantity due to increase in media area, the removal efficiencies obtained for both configurations were divided by their respective surface areas. The results are shown in Table 2. It can be observed that the surface corrected values of the single-pass removal efficiency ( $\alpha$ ) for the pleated media is 27 % higher than that of the plane media. This means that there is an increase in the efficiency not only due to the increase in catalyst quantity but probably also due to the increase in contact time and the possibly the better distribution of irradiance within the media.

Geometry	A (m <sup>2</sup> )	$\alpha/A$ (m <sup>-2</sup> )
Plane	0.040	0.300 ± 0.003
Pleated	0.072	0.380 ± 0.010

**Table 2 : Surface corrected single-pass removal efficiencies of acrylonitrile calculated for the plane and pleated configurations**

Indeed, the contact time between the pollutants and the photocatalytic media and the distribution of irradiance is different in the two geometries. It is assumed that the contact time is globally increased in the pleated geometry. As previously discussed, Destailats *et al.* (Destailats et al., 2012) state that the increase in contact time is as a result of the decreasing velocity of pollutants whilst for Batault (Batault, 2014), the increase in the contact time is as a result of the longer path length travelled by the pollutants. Additionally, they state that for the same average light intensity received on the photocatalytic media (plane and pleated), a modification of the irradiance distribution can also have an influence on the global efficiency of the PCO. These parameters are difficult to measure or confirm experimentally, therefore numerical simulations can be used to provide some information to be able to better connect the increase in efficiency to the change in geometry.

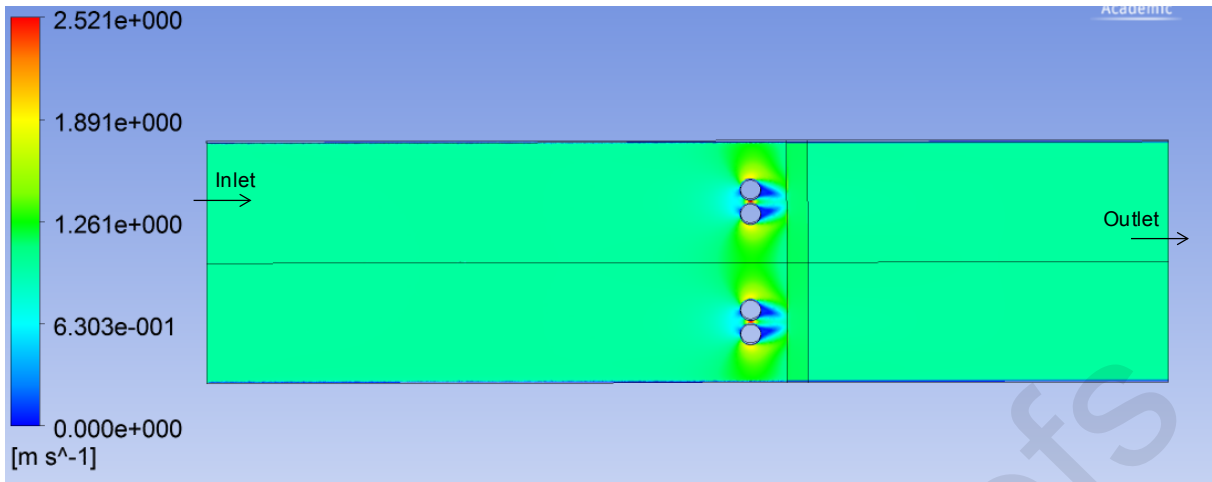
### *3.3 Influence of the media geometry on the single-pass removal efficiency during photocatalytic degradation of acrylonitrile*

To better understand the role of the media geometry in improving the removal efficiencies, numerical simulations were done to investigate the behavior of air flow and light irradiance in the photocatalytic reactor for both configurations.

#### *3.3.1 Fluid dynamics modeling*

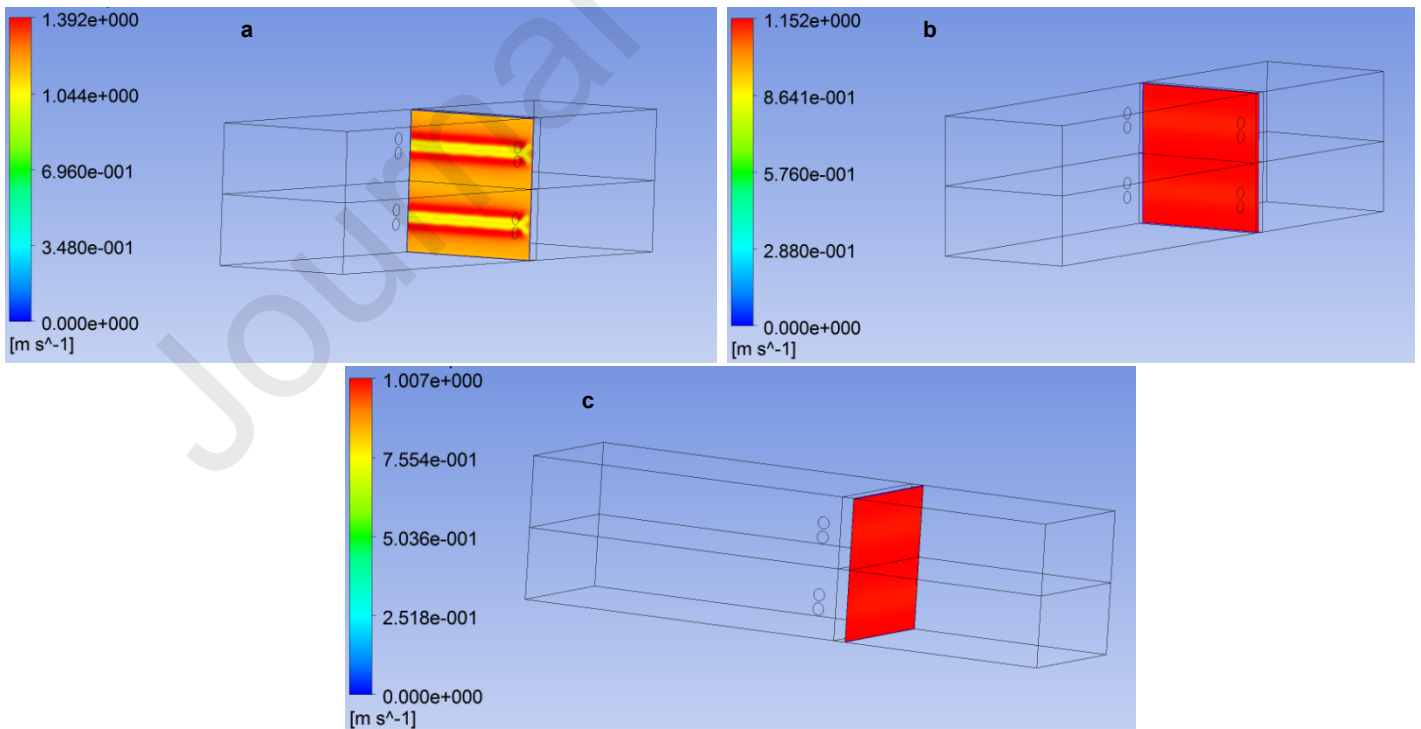
The aim of this section is to be able to describe the behavior of the flow in the reactor and in the media and also determine the contact time within the media. The results for the plane configuration are first discussed followed by those of the pleated configuration.

Fig. 4 shows the results for the flow distribution from the inlet to the outlet of the photocatalytic module along a plane for the plane media geometry. From Fig.4, it is observed that the flow is homogeneous from the inlet until it encounters the lamps where the flow is obliged to move around the lamps. This change in course presented by the lamps, causes zones of higher velocity above and beneath the lamps and zones of lower velocity behind the lamps. However, once inside the media, the flow homogenizes again and remains homogeneous when it exits the media and subsequently the reactor.



**Fig. 4 : Velocity contour showing flow behavior through the reactor in the plane configuration with inlet velocity of  $1\text{m}\cdot\text{s}^{-1}$**

Due to the fact the lamps are quite close to the media (3 cm), this behavior of having zones with higher and lower velocities compared to the inlet velocities is replicated at the inlet of the media as shown in Fig.5a. The range of velocities at the media inlet is  $0.9 - 1.39\text{ m}\cdot\text{s}^{-1}$ . Once inside the media, the flow becomes quite homogeneous as shown in Fig.5b. The range at this distance is  $1.12 - 1.15\text{ m}\cdot\text{s}^{-1}$ . The flow is still homogeneous when it exits the media as shown in Fig.5c and has a range of  $0.98 - 1.0\text{ m}\cdot\text{s}^{-1}$ .



**Fig.5 : Velocity contour showing flow behavior on (a) the surface of the photocatalytic media (b) 8mm distance in media (c) outlet of the media in the plane configuration**

The streamlines were then studied and the results are shown in Fig.6. It shows that the flow is parallel with some small recirculation zones behind the lamps but these are not significant enough to affect entire flow. The streamlines within the media showed that the flow is orthogonal as it moves through the media signifying that the path length within the media is equal to the media thickness.

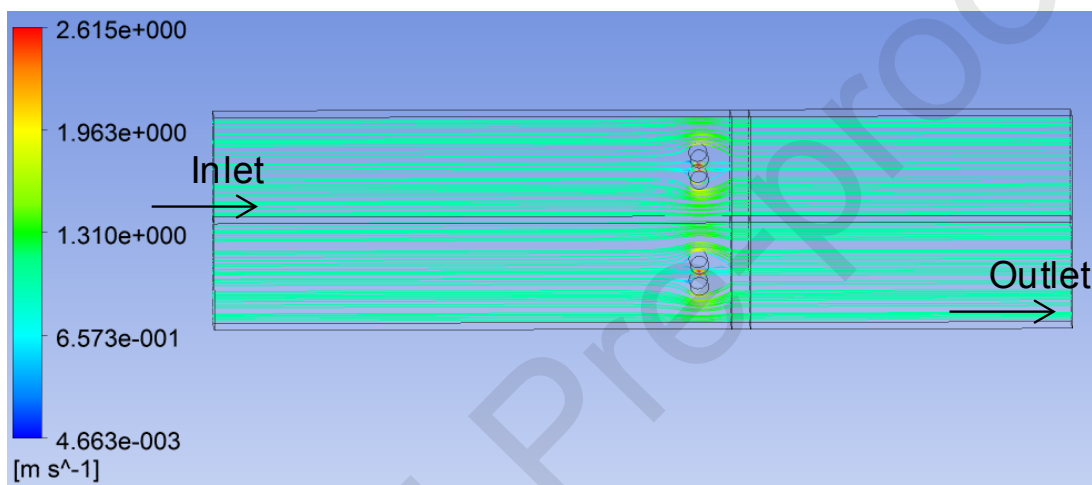


**Fig. 6 : Streamlines through the photocatalytic module in plane media configuration**

To verify the simulation results, the velocity distribution along the height of the reactor at a distance of 8 cm on the x-axis and 6 cm before the media surface was measured experimentally. A Veloport 20 portable air velocity meter was placed in the reactor and the velocity at several distances along the height of the reactor was recorded. Experimental measures were triplicated. As observed in Fig.7, the simulated and experimental results were quite similar signaling that the simulation was quite representative of what was occurring in real conditions.

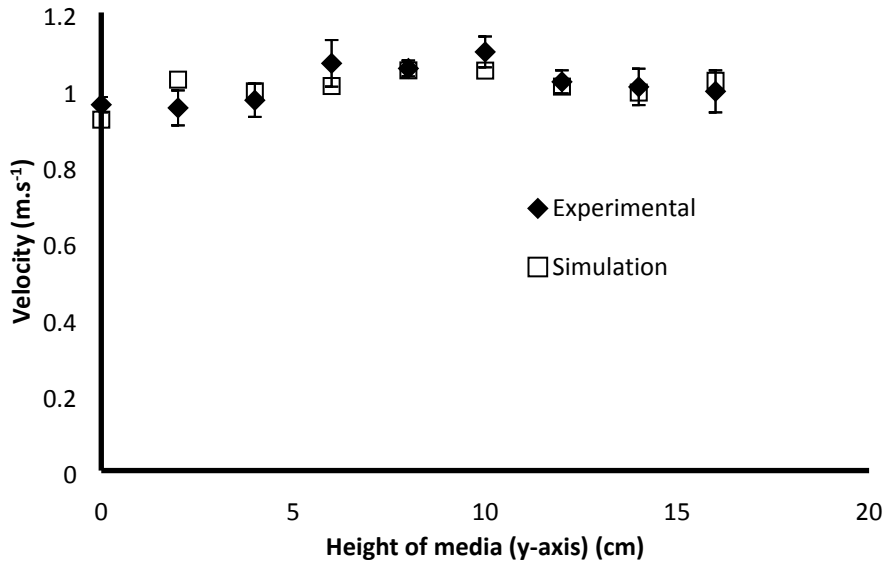


**Fig. 7 : Comparison between simulated and experimental velocity values along the height of reactor at a distance of 6 cm before media**

The average velocity that is received on the media surface and also within the media is calculated to be  $1.14 \text{ m.s}^{-1}$ . This value is about 14% higher than the inlet velocity of  $1 \text{ m.s}^{-1}$ . For fluid flow through a porous medium, the superficial velocity ( $v_0$ ) is the flow rate  $Q$  ( $\text{m}^3.\text{s}^{-1}$ ) divided by the cross-sectional area  $A$  ( $\text{m}^2$ ). In our case, the presence of  $\text{SiO}_2$  fibers and  $\text{TiO}_2$  particles within the photocatalytic media reduces the area available for fluid flow i.e. to conserve fluid continuity with the entering superficial flow, the fluid has to move through a smaller area; hence the velocity within the photocatalytic media ( $v$ ) is greater than that of the superficial velocity. The true velocity ( $v$ ) is related to the superficial velocity by the following expression (Holdich, 2002):

$$v = \frac{v_0}{\varepsilon} \quad (9)$$

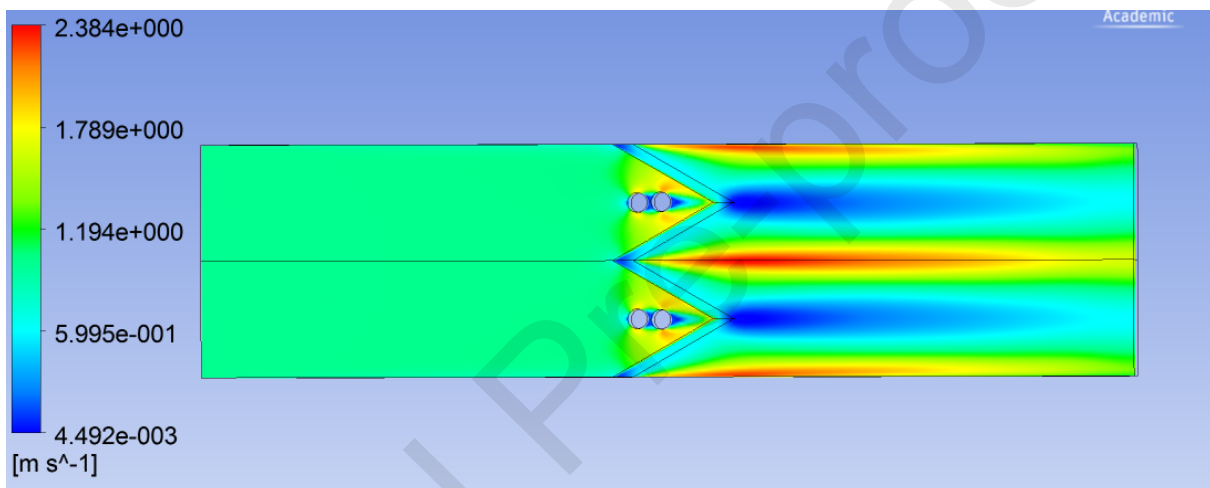
where  $\varepsilon$  is the porosity. Here  $v_0 = 1 \text{ m.s}^{-1}$ ,  $\varepsilon = 0,875$  then  $v = 1/0.875 = 1.14 \text{ m.s}^{-1}$ .

In knowing the average velocity within the media and the path length, the contact time ( $\tau$ ) was then calculated as 15.3 ms using the equation:

$$\tau = \frac{e}{v} \quad (10)$$

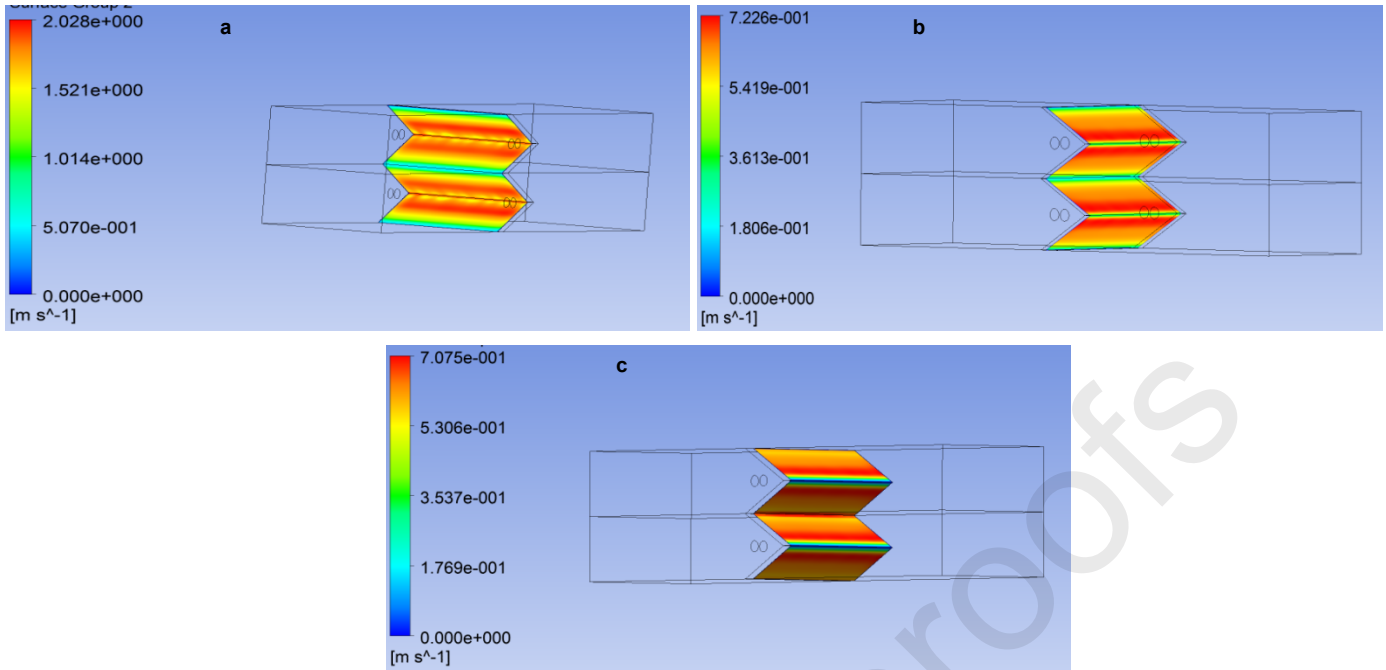
Where  $e$  is the path length is equal to the thickness of the media (m) which is 17.5 mm and  $v$  is the average true velocity in media ( $\text{m}\cdot\text{s}^{-1}$ ).

For the pleated media geometry, the behavior of the flow as it moves across the photocatalytic module is shown in Fig. 8. Similarly to the plane configuration, the flow in the pleated configuration is homogeneous until it encounters the lamps. At this point, the presence of the lamps and the pleats causes the flow to lose its homogeneity. Additionally, as a result of the influence of the presence of the pleats, the flow exiting the media is quite heterogeneous.



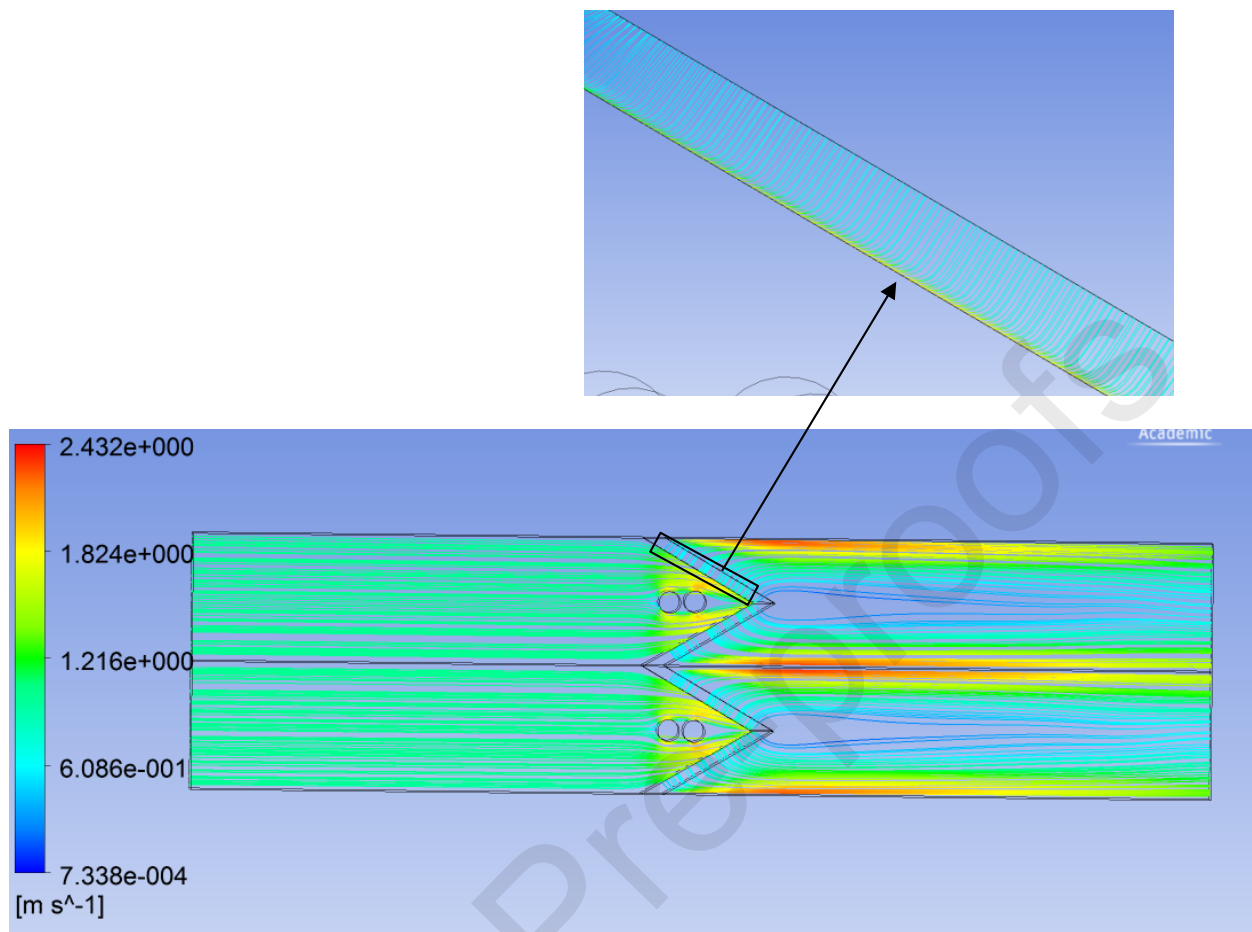
**Fig. 8: Velocity contour showing flow behavior through the reactor in the pleated configuration**

Fig. 9a shows the velocity profile received at the media inlet. It can be observed that the flow is heterogeneously distributed on the surface with the maximum velocities at the regions surrounding the pleat joints. The range on the surface is found to be  $0.07 - 2.03 \text{ m}\cdot\text{s}^{-1}$ . Unlike the plane configuration, the flow does not homogenize within the media as shown in Fig. 9b. The range of velocity 8 mm into the media is found to be  $0.17 - 0.72 \text{ m}\cdot\text{s}^{-1}$ . At the exit of the media the minimum velocities are found at the pleat joints as shown in Fig. 9c and the range of velocities for the entire surface is  $0.0098 - 0.7 \text{ m}\cdot\text{s}^{-1}$ .



**Fig. 9 : Velocity contour showing flow behavior on (a) the surface of the photocatalytic media (b) 8mm distance in media (c) outlet of the media in the pleated configuration**

The streamlines show that the flow is parallel but once it enters the media becomes orthogonal as shown in Fig.10. A closer look at the media shows that the flow enters perpendicularly into the media but at a distance of about 3 mm within the media the flow becomes orthogonal and remains orthogonal until the exit of the media. This means that the path length travelled within the media could be assumed to be equal to the thickness of the media.



**Fig. 10 : Streamlines through the photocatalytic module and media in pleated media configuration**

At the inlet surface of the media, the average velocity received is about  $1.5 \text{ m.s}^{-1}$  and is 32% higher than what is received averagely by the plane configuration. This increase could probably be explained by the fact that presence of the pleats creates a canal effect (which means that area reduces) such that the velocity increases in order to maintain the same flow-rate. However once inside the media the increase in the surface area causes the velocity to be reduced to an average of about  $0.65 \text{ m.s}^{-1}$  which is about 43 % lower than the average velocity within plane configuration. Since the distance travelled (path length) was equivalent to the thickness of the media, the contact time within the pleated media is calculated as 26.9 ms.

### 3.3.2 Radiation field modeling

The objective of this section is to evaluate and compare the distribution of irradiance received within the reactor and media for the two geometry configurations. The simulation results are discussed first for the plane configuration then for the pleated configuration.

The irradiation behavior through the reactor for the plane media geometry is shown in Fig.11. It can be seen that the irradiance is the highest around the lamps but rapidly decays as the distance from the lamps increases. This is attributed to the effect of geometric attenuation which is explained as the reduction in the radiation quantity due to the distance between the point of interest and the source and excludes absorption by any matter present.

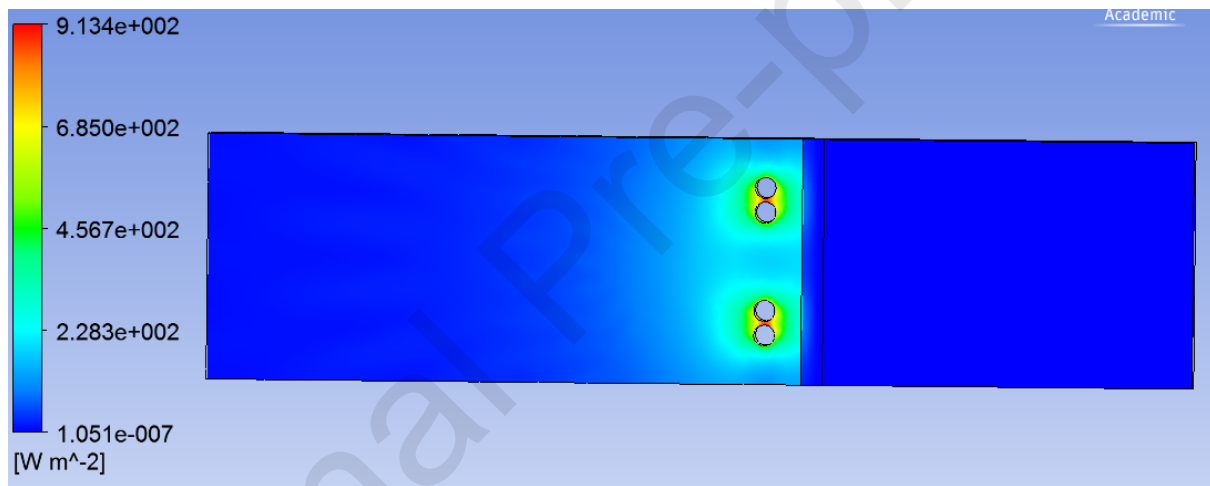


**Fig. 11 : Irradiance contours showing irradiance distribution through reactor for plane media configuration**

The irradiance distribution on the surface of the media was then investigated of which the results are shown in Fig.12a. The irradiance is not homogeneously distributed on the surface, it is highest in the areas found directly behind the lamps but moving away from the lamps, the light irradiance decreases. This behavior is similar to what was observed from the experimental measurements as shown in Fig.12b. It is also observed that the lowest illuminated regions are around the corners.

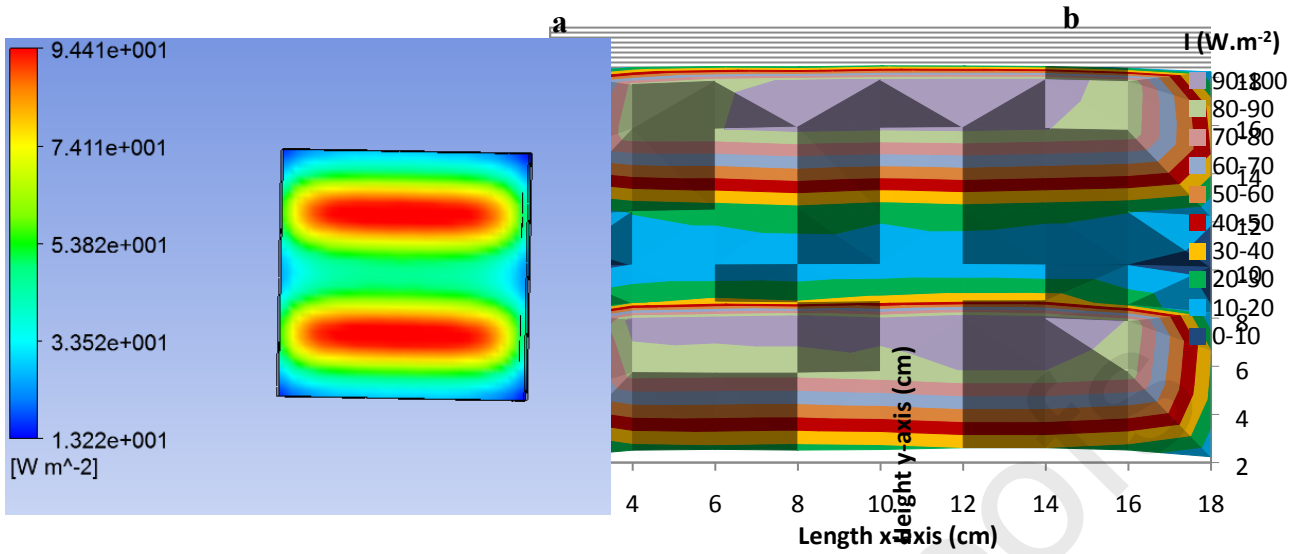


**Fig. 12 : Irradiance distribution on media surface; (a) simulation (b) experimental measurements**

The emissive power of the lamps is a necessary input parameter to attain the desired results during the simulation. As the emissive power is not known in this case, the input value has been approached using values from experimental measurements. Thus to verify the accuracy of the simulation results, the emissive power of the lamps was iteratively changed until the irradiance values that were experimentally measured along the height of the media surface at a distance of 10 cm on the x-axis matched the simulation values. The results are presented in Fig. 13.

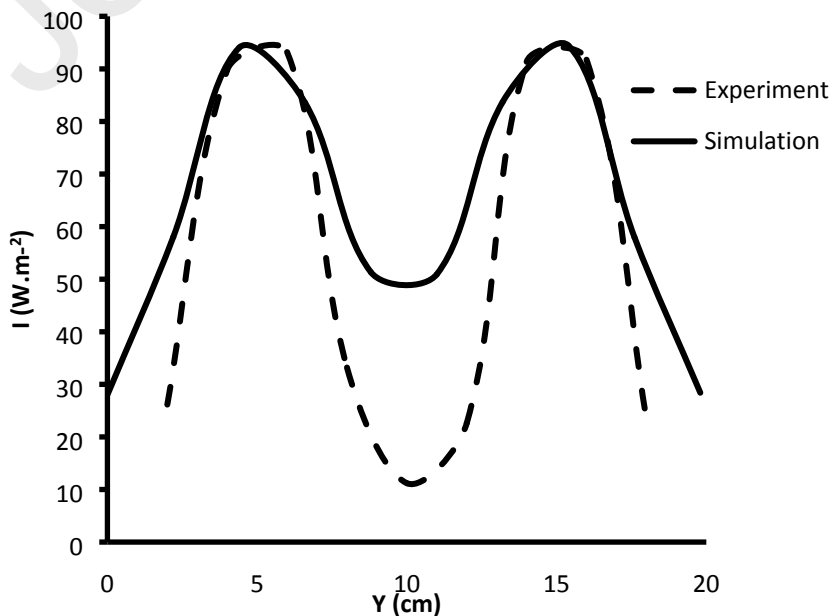


**Fig. 13 : Comparison between simulated and experimental irradiance values along the height of the plane media at a distance of 10 cm along the media length (y-axis)**

It can be observed that the irradiance values increase up to a point then decrease and start to increase again. The highest irradiance values represent the areas on the media directly behind the lamp whilst the lowest values represent the area between the two lamps. From the graph, it is seen that the simulation values are quite similar to the experimental values at highest values or in areas directly behind the lamp. However for the values that represented the region between the two lamps, the simulation values are higher than what was measured experimentally. This difference between the simulated and experimental values could be attributed to the influence of the radiometer that was used for the experimental measurements.

UV radiometers are developed to replicate and preserve an ideal cosine response in order to accurately measure irradiance. However, some of these radiometers may have angular responses that deviate from the ideal cosine response (Larason and Cromer, 2001; Michalsky et al., 1995; Zibordi and Bulgarelli, 2007). When the sensor is located directly in line with the light source a more accurate reading is obtained but once the angle of incidence is increased the error between the ideal cosine response and the detector reading increases and the sensor underestimates the irradiance that is received at that point (Berni et al., 2013; Feister et al., 1997).

For the pleated configuration, the emissive power in the simulation was changed until the average irradiance received on the pleated media surface was similar to that received on the plane media surface.

Once this was done, the irradiance distribution was then studied. Fig.14 shows the irradiance distribution within the reactor. The results presented show that similarly to the plane configuration the irradiance was highest around the lamps and decreased as the distance from the lamps increased due to the effect of geometric attenuation.

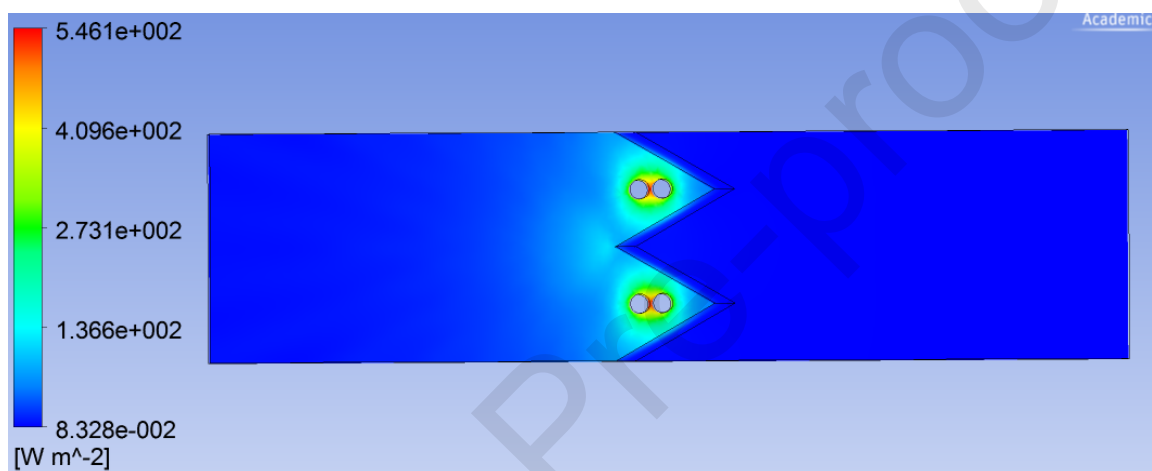


**Fig. 14 : Irradiance contours showing irradiance distribution through reactor for pleated media configuration**

The distribution received on the surface of the media was also studied. First of all, Fig.15a shows that the irradiance is not homogeneously distributed on the surface and secondly that the highest irradiance is found in the areas directly behind the lamps and decreased as the distance from the lamps increased. It is also observed that the region around pleat joints is the lowest illuminated region. This trend is replicated through the media as shown in Fig. 15b and c.

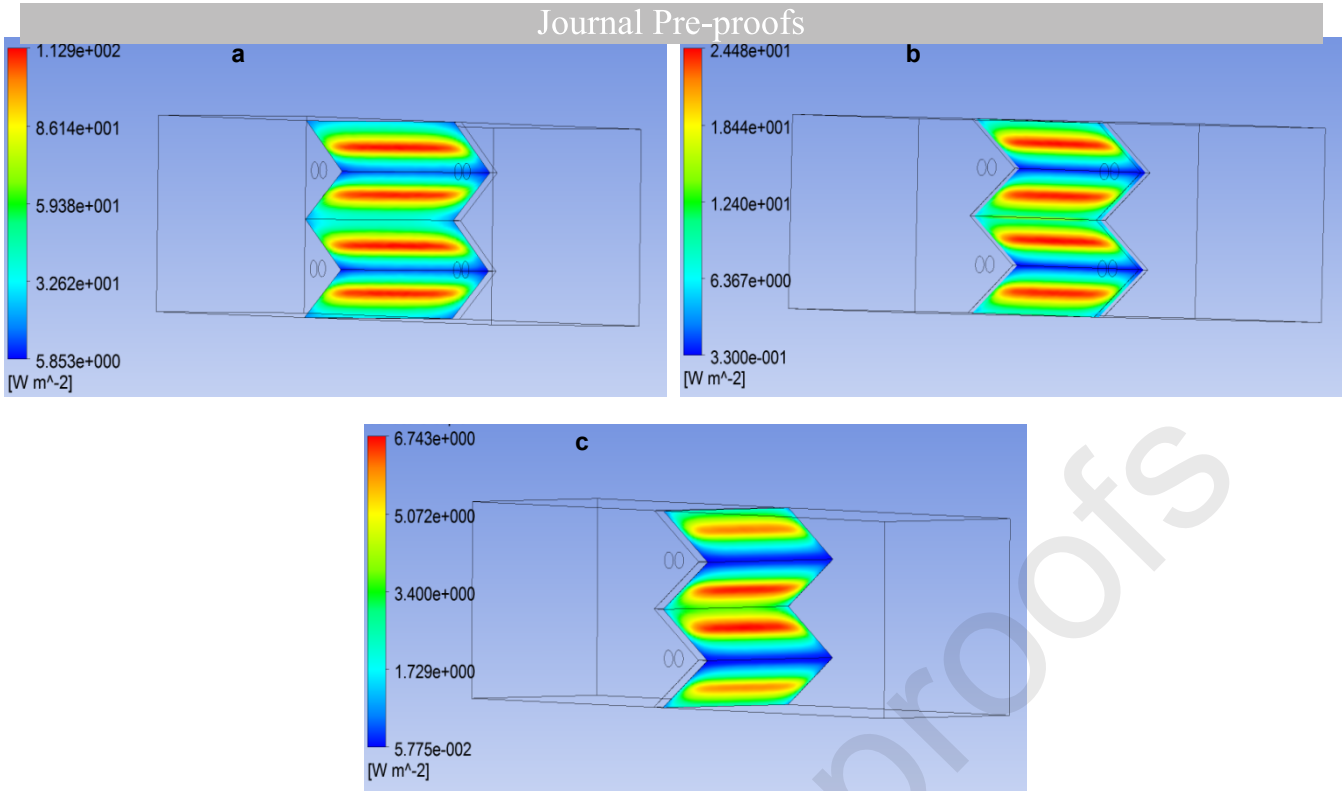


**Fig. 15 : Irradiance contour showing flow behavior on (a) the surface of the photocatalytic media (b) 8mm distance in media (c) outlet of the media in the pleated configuration**

As previously stated, the desired average irradiance on the surface of the media is obtained by controlling the power of the lamp using a variable voltage supply. Thus in order to obtain an average intensity on the pleated media surface that was similar to that of the plane media for the experiments, the variable voltage was adjusted until the highest experimental value corresponded to the highest simulated value. For the simulation, the measurements were taken from across the length of the media at a distance of 10 cm on the height for only one pleat. The highest value was taken as the reference value because this was the value directly in line with the lamp and the plane media results showed that the measurements were most accurate when the sensor was directly in line with the light. The decision was also taken to verify the simulation results only on one pleat due to the difficulty to experimentally measure the irradiance on the entire surface of the pleated media as it was done for the plane. The result of the comparison between the simulated and experimental values is shown in Fig. 16. Here it is observed that the experimental and simulated values are quite similar. This could be probably explained by the

fact that the angle created by the pleats led to a decrease in incident angles which subsequently led to a decrease in the measurements error.

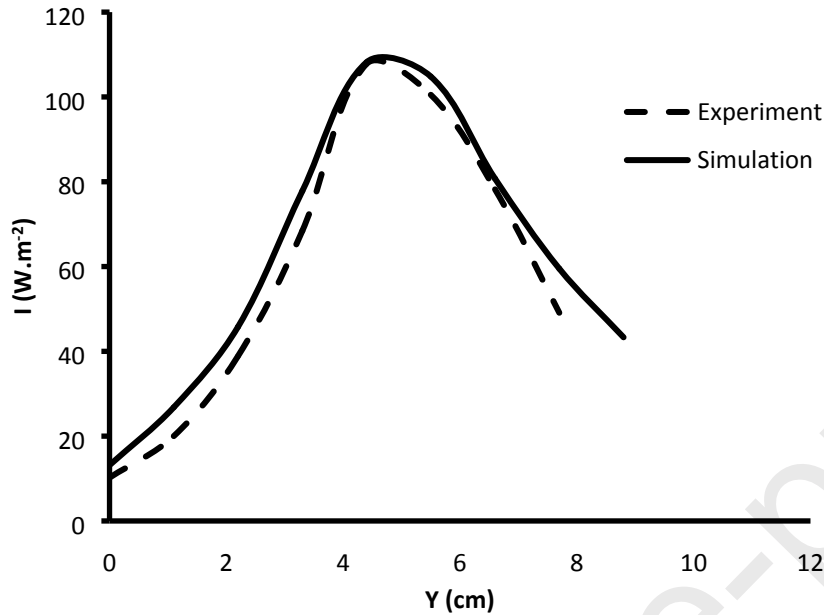


**Fig. 16 : Comparison between simulated and experimental irradiance values along the length of the one pleat at a distance of 10 cm along the media height**

The distribution of irradiance is different for both media geometries and the light intensity is more heterogeneous (bigger range in values) in the pleated than in the plane. Table 3 shows the range in values depending on location in media.

Variable	Geometry	Media inlet	8 mm in media	Media outlet
Irradiance ( $\text{W.m}^{-2}$ )	Plane	13.22 – 94.41	4.38 – 33.47	0.06 -1.03
	Pleated	5.80 -112.90	0.33 -24.50	0.05 – 6.74

**Table 3 : Range of irradiance on different sections within the media**

Simulation results also show that for both media geometry there are regions where the irradiation is quiet low. It can be assumed that the degradation in these regions would be less effective. For the plane media geometry, the lowest irradiated regions are the corners of the

media irrespective of the location (inlet, 8mm within media and outlet) in the media. In the case of the pleated media, the lowest illuminated region is the region around pleat joints. Depending on the location in the media the irradiance changed. Therefore using a criterion range of 0.06  $\text{W.m}^{-2}$  to 13  $\text{W.m}^{-2}$ , it represented 1.5 % of the total surface of the plane media and 18 % of the total pleated media surface.

### 3.3.2.1 *Light distribution within the photocatalytic media*

Monolith photocatalytic media are known to offer low-pressure drop and high catalyst surface area however the light intensity is known to quickly decline through the media (Boyjoo et al., 2017; Sauer and Ollis, 1994). Fig. 17 shows the irradiance profile through the photocatalytic media for both configurations. The irradiance is highest at the media inlet but decreases sharply to 23% at 50% distance within the media for both configurations. At 85% media distance it drops below 1% for the plane media and 3% for the pleated configuration. Beyond this distance the media is not sufficiently illuminated and is subjected to operation under dark conditions. Wang *et al.* (Wang et al., 2014) found similar results when they simulated the irradiance profile through a cordierite ceramic monolithic media with a thickness of 25.4 mm. In plotting a graph of the dimensionless UV flux to distance they found that at a distance of 3.2 mm the UV light intensity decreased to 30 % of the incoming flux and to 1 % at a distance of 9.5 mm. These results suggest that a shorter media width would be preferable to reduce the dark zones or the provision of lamps on both sides of the photocatalytic media to allow a better utilization of the media

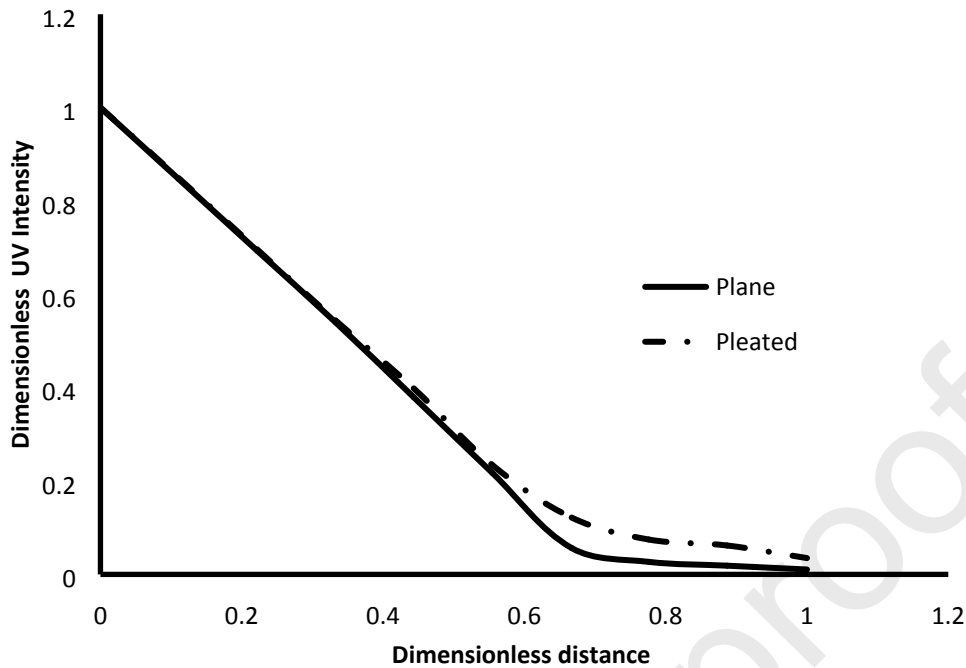


**Fig. 17 : Irradiance profile within photocatalytic media for plane and pleated configurations**

### 3.4 Calculation of effective-surface single-pass removal efficiencies

In section 3.2, the surface corrected single-pass removal efficiencies ( $\alpha/m^2$ ) were found to be 27% higher for the pleated geometry than for the plane geometry as shown previously in Table 2. As previously discussed, the light intensity received on and within the media remains the same and the simulations show a 76 % increase in contact time by using the pleated media geometry. Thus, ideally if all parameters are constant for both configuration and only the contact increases, we expect that the surface corrected single-pass removal efficiencies ( $\alpha/m^2$ ) obtained from the experiments would be similar to this number but the experiments showed a much lower improvement of 27 %. Two hypotheses could be proposed to explain this performance:

(i) It was observed that the lowest region of illumination where the media would be operating under near dark conditions and would not be very effective represented 18 % of the total media surface compared to the 1.5 % in the plane media. This subsequently means that effective surface of the pleated media was further decreased. If the surface corrected single-pass removal efficiency ( $\alpha/m^2$ ) is calculated considering the new “efficient surface” for both plane and pleated media, it is observed that it is 48 % higher for the pleated geometry than for the plane geometry. Quantitative results are presented in Table 4.

<b>Geometry</b>	<b>A' (m<sup>2</sup>)</b>	<b><math>\alpha</math></b>	<b><math>\alpha/A'</math> (m<sup>-2</sup>)</b>
<b>Plane</b>	0.039	0.01203 ± 0.00011	0.308 ± 0.003
<b>Pleated</b>	0.059	0.02742 ± 0.00074	0.46 ± 0.01

**Table 4 : Surface corrected single-pass removal efficiencies ( $\alpha/m^2$ ) of acrylonitrile calculated for the plane and pleated configurations and the corrected surface areas (A') for each configuration**

(ii) It was also shown in the simulation that the flow and irradiance distribution within the pleated geometry was more heterogeneous (bigger range in values) than the plane geometry (Table 5). This means that even though the global average velocity was decreased and the contact time was higher within the pleated media, the higher level of heterogeneity could explain why the  $\alpha$  values were lower than expected for the pleated configuration. Some authors have concluded that when light intensity distribution of the surface is homogenous it increases the overall photonic efficiency and better reaction rates are achieved whilst with heterogeneous distribution, areas of high light intensity will experience low photonic efficiency as a possible result of

the electron hole recombination (Kozlov and Vorontsov, 2011; Martín-Sómer et al., 2017).

Variable	Geometry	Media inlet	8 mm in media	Media outlet
Velocity (m.s <sup>-1</sup> )	Plane	0.9 - 1.39	1.12 -1.15	0.98 - 1.0
	Pleated	0.07 - 2.03	0.17 - 0.72	0.0098 - 0.7
Irradiance (W.m <sup>-2</sup> )	Plane	13.22 – 94.41	4.38 – 33.47	0.06 -1.03
	Pleated	5.80 -112.90	0.33 -24.50	0.05 – 6.74

**Table 5 : Range of velocities and irradiance on different sections within the media**

Conclusively, the use of pleated media geometry improves the degradation efficiency by decreasing the velocity of pollutants within the media and consequently increasing the contact time between the pollutants and the media. However, the more heterogeneous distribution of the velocity in the pleated media counteracts the influence of the contact time. Additionally, even though the average the light intensity on the media is the same for both media, the more heterogeneous distribution in the pleated geometry also hinders the effect of increase in contact time.

#### 4 Conclusions

In this work, the influence of the change in media geometry on the degradation of acrylonitrile, a pollutant present in hospital ORs was studied. The experiments were performed using plane and pleated media geometries placed in a 420-L multi-pass laboratory reactor. The use of a model developed by Dumont and Héquet enabled the calculation of a performance indicator, the single pass removal efficiency. This quantitative descriptor enabled the study of the influence of the change in media geometry on the degradation of acrylonitrile.

The experimental results showed that under similar experimental conditions, the single-pass removal efficiency was increased when the pleated media geometry was used compared to the

plane media geometry. The use of CFD allowed the simulation of velocity and irradiance distribution at the media level for both geometries that otherwise would have been more difficult to achieve experimentally. The results of the air flow and irradiance distribution obtained from simulation enabled the conclusion that the more heterogeneous distribution of velocity and light intensity counteracted and hindered the effect of the increase in contact time.

CFD simulations helped to highlight important behavior with respect to flow and the irradiance in a photocatalytic unit and could be useful to help investigate configurations that could improve the contact time and irradiance but also better homogeneity of these variables in the media. CFD could also be further used to study species transport and chemical reaction kinetics that would help to strengthen predictive capabilities and lessen the number of experiments thus consequently providing an economic advantage.

### **Acknowledgements**

The authors would like to express their gratitude to ATA Medical and IMT Atlantique for their financial support and also to Eric Chevrel, Patrick Brion, Francois-Xavier Blanchet, Yvan Gouriou and Katell Chaillou for their invaluable technical assistance and to Eric Dumont for his help with the modeling.

### **5 References**

ANSYS Inc., 2013. Ansys CFX Solver Modeling Guide, 14.5. ed. Canonsburg.

- Ao, C.H.H., Lee, S.C.C., Yu, J.Z.Z., Xu, J.H.H., 2004. Photodegradation of formaldehyde by photocatalyst TiO<sub>2</sub>: effects on the presences of NO, SO<sub>2</sub> and VOCs. *Appl. Catal. B Environ.* 54, 41–50.
- Barrett, W.L., Garber, S.M., 2003. Surgical smoke: a review of the literature. *Surg. Endosc. Other Interv. Tech.* 17, 979–987. <https://doi.org/10.1007/s00464-002-8584-5>
- Batault, F., 2014. Influence de l'adsorption et des paramètres opératoires sur le traitement photocatalytique de composés organiques volatils en mélange dans les conditions de l'air intérieur. <http://www.theses.fr>. Lille 1.
- Batault, F., Héquet, V., Raillard, C., Thévenet, F., Locoge, N., Le Coq, L., 2017. How chemical and physical mechanisms enable the influence of the operating conditions in a photocatalytic indoor air treatment device to be modeled. *Chem. Eng. J.* 307, 766–775. <https://doi.org/10.1016/j.cej.2016.08.118>
- Bergeron, V., Reboux, G., Poirot, J.L., Laudinet, N., 2007. Decreasing Airborne Contamination Levels in High-Risk Hospital Areas Using a Novel Mobile Air-Treatment Unit. *Infect. Control Hosp. Epidemiol.* 28, 1181–1186. <https://doi.org/10.1086/520733>
- Berni, L.Â., Vilela, W.A., Beloto, A.F., de Sena, F.O., 2013. System for measuring the angular response of radiometers, in: Martins Costa, M.F.P.C. (Ed.), . International Society for Optics and Photonics, p. 87852F. <https://doi.org/10.1117/12.2019888>
- Birnie, M., Riffat, S., Gillott, M., 2006. Photocatalytic reactors: design for effective air purification. *Int. J. Low-Carbon Technol.* 1, 47–58. <https://doi.org/10.1093/ijlct/1.1.47>
- Boyjoo, Y., Ang, M., Pareek, V., 2014. Lamp emission and quartz sleeve modelling in slurry photocatalytic reactors. *Chem. Eng. Sci.* 111, 34–40. <https://doi.org/10.1016/J.CES.2014.02.023>
- Boyjoo, Y., Ang, M., Pareek, V., 2013. Some aspects of photocatalytic reactor modeling using computational fluid dynamics. *Chem. Eng. Sci.* 101, 764–784. <https://doi.org/10.1016/J.CES.2013.06.035>
- Boyjoo, Y., Sun, H., Liu, J., Pareek, V.K., Wang, S., 2017. A review on photocatalysis for air treatment: From catalyst development to reactor design. *Chem. Eng. J.* 310, 537–559. <https://doi.org/10.1016/J.CEJ.2016.06.090>
- Chen, W., Zhang, J.J., 2016. Photocatalytic Oxidation of Multi-Component Systems – An Investigation Using Toluene/Ethylbenzene, Octane/Decane/Dodecane and Formaldehyde/Acetaldehyde. *J. Adv. Oxid. Technol.* 11, 163–173. <https://doi.org/10.1515/jaots-2008-0123>
- Chong, S., Wang, S., Tade, M., Ang, H.M., Pareek, V., 2011. Simulations of photodegradation of toluene and formaldehyde in a monolith reactor using computational fluid dynamics. *AIChE J.* 57, 724–734. <https://doi.org/10.1002/aic.12295>
- Dascalaki, E.G., Lagoudi, A., Balaras, C.A., Gaglia, A.G., 2008. Air quality in hospital operating rooms. *Build. Environ.* 43, 1945–1952. <https://doi.org/10.1016/j.buildenv.2007.11.015>

- Destailats, H., Sleiman, M., Sullivan, D.P., Jacquioid, C., Sablayrolles, J., Molins, L., 2012. Key parameters influencing the performance of photocatalytic oxidation (PCO) air purification under realistic indoor conditions. *Appl. Catal. B Environ., Heterogeneous catalysis: from electronic processes to Photocatalysis. A special issue dedicated to Jean-Marie Herrmann* 128, 159–170. <https://doi.org/10.1016/j.apcatb.2012.03.014>
- Dillert, R., Stötzner, J., Engel, A., Bahnemann, D.W., 2012. Influence of inlet concentration and light intensity on the photocatalytic oxidation of nitrogen(II) oxide at the surface of Aeroxide® TiO<sub>2</sub> P25. *J. Hazard. Mater.* 211–212, 240–246. <https://doi.org/10.1016/J.JHAZMAT.2011.11.041>
- Dumont, E., Héquet, V., 2017. Determination of the Clean Air Delivery Rate (CADR) of Photocatalytic Oxidation (PCO) Purifiers for Indoor Air Pollutants Using a Closed-Loop Reactor. Part I: Theoretical Considerations. *Molecules* 22. <https://doi.org/10.3390/molecules22030407>
- Feister, U., Grewe, R., Gericke, K., 1997. A method for correction of cosine errors in measurements of spectral UV irradiance. *Sol. Energy* 60, 313–332. [https://doi.org/10.1016/S0038-092X\(97\)00030-3](https://doi.org/10.1016/S0038-092X(97)00030-3)
- Holdich, R., 2002. Fluid flow through porous media, in: *Fundamentals of Particle Technology*. Midland Information Technology and Publishing, Leicestershire, pp. 21–28.
- Kozlov, D. V., Panchenko, A.A., Bavykin, D. V., Savinov, E.N., Smirniotis, P.G., 2003. Influence of humidity and acidity of the titanium dioxide surface on the kinetics of photocatalytic oxidation of volatile organic compounds. *Russ. Chem. Bull.* 52, 1100–1105. <https://doi.org/10.1023/A:1024796905146>
- Kozlov, D. V., Vorontsov, A. V., 2011. Development of Multi-Stage Photocatalytic Reactors for Air Purification.
- Larason, T.C., Cromer, C.L., 2001. Sources of Error in UV Radiation Measurements. *J. Res. Natl. Inst. Stand. Technol.* 106, 649–56. <https://doi.org/10.6028/jres.106.030>
- Le, T.S., Dao, T.H., Nguyen, D.C., Nguyen, H.C., Balikhin, I.L., 2015. Air purification equipment combining a filter coated by silver nanoparticles with a nano-TiO<sub>2</sub> photocatalyst for use in hospitals. *Adv. Nat. Sci. Nanosci. Nanotechnol.* 6, 015016. <https://doi.org/10.1088/2043-6262/6/1/015016>
- Martín-Sómer, M., Pablos, C., van Grieken, R., Marugán, J., 2017. Influence of light distribution on the performance of photocatalytic reactors: LED vs mercury lamps. *Appl. Catal. B Environ.* 215, 1–7. <https://doi.org/10.1016/J.APCATB.2017.05.048>
- Maudhuit, A., Raillard, C., Héquet, V., Le Coq, L., Sablayrolles, J., Molins, L., 2011. Adsorption phenomena in photocatalytic reactions: The case of toluene, acetone and heptane. *Chem. Eng. J., Environmental Nanotechnology* 170, 464–470. <https://doi.org/10.1016/j.cej.2011.02.040>
- Michalsky, J.J., Harrison, L.C., Berkheiser, W.E., 1995. Cosine response characteristics of some radiometric and photometric sensors. *Sol. Energy* 54, 397–402. [https://doi.org/10.1016/0038-092X\(95\)00017-L](https://doi.org/10.1016/0038-092X(95)00017-L)

- Mohseni, M., Taghipour, F., 2004. Experimental and CFD analysis of photocatalytic gas phase vinyl chloride (VC) oxidation. *Chem. Eng. Sci.* 59, 1601–1609. <https://doi.org/10.1016/j.ces.2004.01.017>
- Passalía, C., Alfano, O.M., Brandi, R.J., 2012. A methodology for modeling photocatalytic reactors for indoor pollution control using previously estimated kinetic parameters. *J. Hazard. Mater.* 211–212, 357–365. <https://doi.org/10.1016/J.JHAZMAT.2011.10.007>
- Perraud, M., Nicolle, M.C., Chiarello, E., Tissot Guerraz, F., Cetre, J.C., Sepetjan, M., 1992. Air filtration and prevention of aspergillary pneumopathies. Preliminary comparative study of two mobile units for bacteriological air purification with recycling. *Nouv. Rev. Fr. Hematol.* 34, 295–299.
- Pichat, P., 2010. Some views about indoor air photocatalytic treatment using TiO<sub>2</sub>: Conceptualization of humidity effects, active oxygen species, problem of C1–C3 carbonyl pollutants. *Appl. Catal. B Environ.* 99, 428–434. <https://doi.org/10.1016/J.APCATB.2010.07.022>
- Queffeuou, A., Geron, L., Schaer, E., 2010. Prediction of photocatalytic air purifier apparatus performances with a CFD approach using experimentally determined kinetic parameters. *Chem. Eng. Sci.* 65, 5067–5074. <https://doi.org/10.1016/J.CES.2010.05.024>
- Raillard, C., Héquet, V., Le Cloirec, P., Legrand, J., 2004. Kinetic study of ketones photocatalytic oxidation in gas phase using TiO<sub>2</sub>-containing paper: effect of water vapor. *J. Photochem. Photobiol. A Chem.* 163, 425–431.
- Raillard, C., Maudhuit, A., Héquet, V., Le Coq, L., Sablayrolles, J., Molins, L., 2014. Use of experimental designs to establish a kinetic law for a gas phase photocatalytic process. *Int. J. Chem. React. Eng.* 12, 113. <https://doi.org/10.1515/ijcre-2014-0012>
- Romero-Vargas Castrillón, S., Ibrahim, H., de Lasa, H., 2006. Flow field investigation in a photocatalytic reactor for air treatment (Photo-CREC–air). *Chem. Eng. Sci.* 61, 3343–3361. <https://doi.org/10.1016/J.CES.2005.11.039>
- Rosenbaum, R.A., Benyo, J.S., O'Connor, R.E., Passarello, B.A., Williams, D.R., Humphrey, B.D., Ross, R.W., Berry, J.M., Krebs, J.G., 2004. Use of a portable forced air system to convert existing hospital space into a mass casualty isolation area. *Ann. Emerg. Med.* 44, 628–634. <https://doi.org/10.1016/j.annemergmed.2004.03.012>
- Salvadó-Estivill, I., Hargreaves, D.M., Puma, G.L., 2007. Evaluation of the intrinsic photocatalytic oxidation kinetics of indoor air pollutants. *Environ. Sci. Technol.* 41, 2028–35.
- Sauer, M.L., Ollis, D.F., 1994. Acetone Oxidation in a Photocatalytic Monolith Reactor. *J. Catal.* 149, 81–91. <https://doi.org/10.1006/JCAT.1994.1274>
- Schoenleber, T., Gbaguidi Haore, H., Jeunet, L., Talon, D., 2007. Évaluation d'un dispositif mobile de décontamination pour la maîtrise de l'air au bloc opératoire. *Hygienes* 15, 158–164.
- Sleiman, M., Conchon, P., Ferronato, C., Chovelon, J.-M., 2009. Photocatalytic oxidation of toluene at indoor air levels (ppbv): Towards a better assessment of conversion, reaction

- intermediates and mineralization. *Appl. Catal. B Environ.* 86, 159–165.
- Wang, X., Tan, X., Yu, T., 2014. Modeling of Formaldehyde Photocatalytic Degradation in a Honeycomb Monolith Reactor Using Computational Fluid Dynamics. *Ind. Eng. Chem. Res.* 53, 18402–18410. <https://doi.org/10.1021/ie5016427>
- Whyte, H.E., Raillard, C., Subrenat, A., Hequet, V., 2018. Photocatalytic oxidation of isoflurane, an anesthetic gas: the influence of operating parameters. *Chem. Eng. J.* <https://doi.org/10.1016/j.cej.2018.07.059>
- Ye, X., Chen, D., Gossage, J., Li, K., 2006. Photocatalytic oxidation of aldehydes: Byproduct identification and reaction pathway. *J. Photochem. Photobiol. A Chem.* 183, 35–40. <https://doi.org/10.1016/j.jphotochem.2006.02.019>
- Yu, Q.L., Brouwers, H.J.H., 2009. Indoor air purification using heterogeneous photocatalytic oxidation. Part I: Experimental study. *Appl. Catal. B Environ.* 92, 454–461. <https://doi.org/10.1016/j.apcatb.2009.09.004>
- Zibordi, G., Bulgarelli, B., 2007. Effects of cosine error in irradiance measurements from field ocean color radiometers. *Appl. Opt.* 46, 5529. <https://doi.org/10.1364/AO.46.005529>

### **Declaration of interests**

The authors declare that they have no known competing financial interests or personal relationships that could have appeared to influence the work reported in this paper.

Journal Pre-proofs